




Cite this: DOI: 10.1039/d5ma00601e

Layer-by-layer growth of graphene oxide multilayers using robust interlayer linking chemistry. 2 Zr–bissulfates

Neelanjana Mukherjee,^a Nancy S. Muyanjan^b and G. J. Blanchard  ^{★a}

We report on the facile layer-by-layer growth of graphene oxide sulfate (GO-S) multilayer structures. The layers are bonded to a modified planar silica support using Zr⁴⁺ ions. Optical ellipsometry shows step-by-step layer growth with layer thickness consistent with that expected from molecular mechanics calculations. The reaction to form Zr–bissulfate linkages is facile, with multistep layer deposition occurring within six to ten minutes per layer. The GO-S layers can be deposited directly on GO-S underlayer(s) or interlayer spacers can be incorporated to control the spacing with GO-S layers. X-ray photoelectron spectroscopy (XPS) data provides information on the density of the sulfonated groups present at the graphene oxide surface and on the Zr : S ratio. This is the first report we are aware of that demonstrates robust layer-by-layer growth of graphene oxide structures.

Received 6th June 2025,
Accepted 7th August 2025

DOI: 10.1039/d5ma00601e

rsc.li/materials-advances

Introduction

The discovery of graphene, two-dimensional sheets of carbon atoms, has proven to be of great importance for both fundamental and practical reasons. Graphene exhibits favorable physical and electronic properties, and this material has been explored extensively due to its two-dimensional nature and electronic structure. Graphite is a three-dimensional allotrope of carbon that is formed by the stacking of many layers of graphene. The forces responsible for the layered structure of graphite are inter-layer van der Waals interactions. Among the notable properties of graphite is its ability to allow for the intercalation of various species in the gallery spaces between individual graphene layers. The lubricating properties of graphite are also thought to be related to van der Waals inter-layer interactions. While such inter-layer interactions are useful and important, there are other applications for which stronger inter-layer bonding is required.

Graphene can be oxidized to produce two-dimensional sheets containing epoxide, alcohol, aldehyde and carboxylic acid functionalities, and these functionalities have proven to be useful not only for the modification of the layer properties but also as chemically reactive sites for further functionalization. Indeed, there is a rich literature on its use in areas ranging

from catalysis to tissue engineering and biomedical applications.^{1–12} We have become interested in graphene oxide because of its ability to be formed into robust multilayer structures with explicit control over number of layers and inter-layer spacing as well as chemically-derived robustness compared to other structures formed by physical deposition such as aerosol, spin coating or Langmuir–Blodgett deposition.

Graphene oxide (GO) is dispersible in water and other organic solvents. Because of its tunable physical and chemical properties, GO is interesting for a wide range of applications such as in electronic and electrochemical devices, energy conversion and storage, and biosensors.¹³ Many of these applications require that morphologically well-defined GO single-layer sheets can be deposited one over the other on large-area substrates.¹⁴ Unfortunately, it is challenging to control GO morphology in thin layers, and methods such as spin-coating or drop-casting offer poor morphological control.¹⁵

Many methods have been devised for the formation of thin layers, including Langmuir–Blodgett deposition,^{16–18} covalent^{19–25} and ionic^{26–48} layer growth, and electrostatic binding,^{45,46} and the layer-by-layer growth of graphene-based systems is also well-established.^{49,50} The choice of layer deposition methodology depends on the support on which the layers are formed and on the desired properties of the resulting thin film materials. Of the methods listed above, layer-by-layer deposition of films affords a high level of control over composition and orientation relative to the support. Both properties can be critical to the macroscopic properties of the resulting system. Gaining the ability to design and construct organized multilayer assemblies with significant control over their

^a Michigan State University, Department of Chemistry, 578 S. Shaw Lane, East Lansing, MI 48824, USA. E-mail: blanchard@chemistry.msu.edu; Tel: +1 517 353 1105

^b Michigan Center for Materials Characterization, University of Michigan, College of Engineering, Ann Arbor, MI 48109, USA



macroscopic properties enables the advancement of a broad range of science and technology.

There is a wide range of chemistry that can be brought to bear on the regular growth of multilayer assemblies. Metal-bisphosphonate chemistry has been used extensively and commonly to produce robust multilayer interfacial materials because of its simplicity and versatility.^{26–44} However, metal bisphosphonate chemistry may not be well suited for all interfacial applications and, multiple different interlayer linking strategies have been demonstrated. Among these alternative linking strategies are those developed are the use of sulfate or sulfonate complexation with various metal ions.^{51–53} We report here on the formation of graphene oxide sulfate (S-GO) multilayers using Zr-sulfate (ZS) interlayer linking chemistry to achieve rapid, robust and well-controlled layer-by-layer growth of on silicon and silica surfaces.

Experimental section

Reagents and materials

Graphite, sodium nitrate (NaNO_3 , $\geq 99.0\%$), sulfuric acid (H_2SO_4 , $95.0\text{--}98.0\%$), potassium permanganate (KMnO_4 , $\geq 99.0\%$), zirconyl chloride octahydrate ($\text{ZrOCl}_2 \cdot 8\text{H}_2\text{O}$, 98%), anhydrous acetonitrile (CH_3CN anhydrous, 99.8%), chlorosulfonic acid (ClSO_3H , 99%), chloroform (CHCl_3 , $\geq 99.8\%$), hydroquinone ($\text{C}_6\text{H}_4(\text{OH})_2$, $\geq 99.5\%$) and ethanol were purchased from Sigma-Aldrich. Hydrogen peroxide (H_2O_2 , 30% in water) was purchased from Fisher Scientific. All reagents were used as received, without further purification. Silicon wafers were purchased from University Wafer. Glass slides (silica) were purchased from VWR International, LLC. Ultrapure Milli-Q water ($18\text{ M}\Omega$) was supplied by a Millipore system and used in all experiments. Glassware was rinsed with Milli-Q water before use.

GO synthesis and S-GO synthesis

GO was synthesized by a modification of the Hummers' method.³⁶ Graphite (0.5 g) was mixed with 23 mL of sulfuric acid in a beaker and stirred on an ice bath. NaNO_3 (0.5 g) was then added, followed by KMnO_4 (3 g). The mixture was brought to 35°C and stirred for 2 h . The mixture was then cooled in an ice bath while 55 mL water was slowly added such that the temperature of the reaction mixture was kept below 10°C . Five mL of H_2O_2 (30% in water) was then slowly added until no more gas evolution was observed. Finally, the mixture was filtered under vacuum and the filter cake was redispersed in 25 mL of anhydrous CH_3CN . The synthesized GO (in CH_3CN) was sulfonated by the addition of $333\text{ }\mu\text{L}$ of ClSO_3H in a fume hood. The mixture was stirred for 10 minutes to ensure that the mixture became homogenous. The S-GO stock solution was covered with parafilm and was ready for use.

Surface preparation

Both silica and silicon substrates were cleaned in piranha solution ($3:1\text{ H}_2\text{SO}_4:\text{H}_2\text{O}_2$, Caution: strong oxidizer!) for 10 minutes , rinsed with Milli-Q water and dried under a stream of N_2 prior to layer deposition.

Layer deposition

The oxidized silicon and silica substrates were directly sulfonated using ClSO_3H in chloroform in a fume hood. After 10 minutes , the substrates were immersed in Milli-Q water before use. The substrates were zirconated by immersion in a 5 mM solution of ZrOCl_2 in ethanol (aqueous, $60\%\text{ v/v}$) for 10 minutes . For the first layer, the zirconated substrates were immersed in the S-GO solution ($\sim 0.2\text{ M}$) for 20 minutes . From second layer onward, the resulting substrates were first immersed ZrOCl_2 solution for 10 minutes , then in 0.2 mM hydroquinone in CH_3CN solution (sulfonated using $0.3\text{ }\mu\text{L ClSO}_3\text{H}$) for 10 minutes , then in ZrOCl_2 solution again for 10 minutes , and lastly, in S-GO solution for 20 minutes . After immersion in S-GO solution, the resulting surfaces would be washed with anhydrous acetonitrile, followed by water and dried with a stream of N_2 before characterization (Fig. 1 and 2).

Optical null ellipsometry

Layer thicknesses were measured using an optical null ellipsometer (M-44, J. A. Woollam Co., Inc.) operated over the wavelength range of 400 nm to 675 nm . The software used for data acquisition and reduction to obtain self-consistent values of $n(\lambda)$ and $k(\lambda)$ was WVASE32 (Woollam Co. Inc.).

UV-visible spectroscopy

A CARY model 4000 spectrometer was used to collect absorption spectra of the multilayer structures. Spectral resolution was 2 nm and the aperture of the transmission measurements was $1\text{ mm} \times 4\text{ mm}$ for all measurements.

Scanning electron microscopy

A JEOL 7500F (field emission emitter) scanning electron microscope (JEOL Ltd., Tokyo, Japan) was used to collect SEM images. SMILE VIEW Map software (developed by JEOL) was used for image processing and analysis. The samples were coated with osmium ($\sim 10\text{ nm}$ thickness) in a Tennant20 osmium CVD (chemical vapor deposition) coater (Meiwafosis Co., Ltd, Osaka, Japan), and were mounted on aluminum stubs using carbon suspension cement (SPI Supplies, West Chester, PA) and epoxy glue (System Three Quick Cure 5 from System Three Resins, Inc., Auburn, WA).

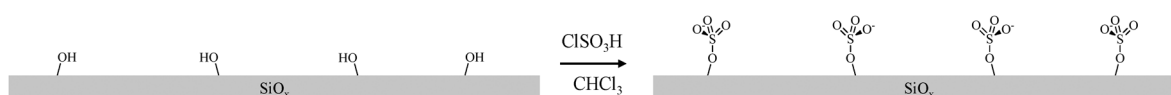


Fig. 1 Schematic of silica surface functionalization.



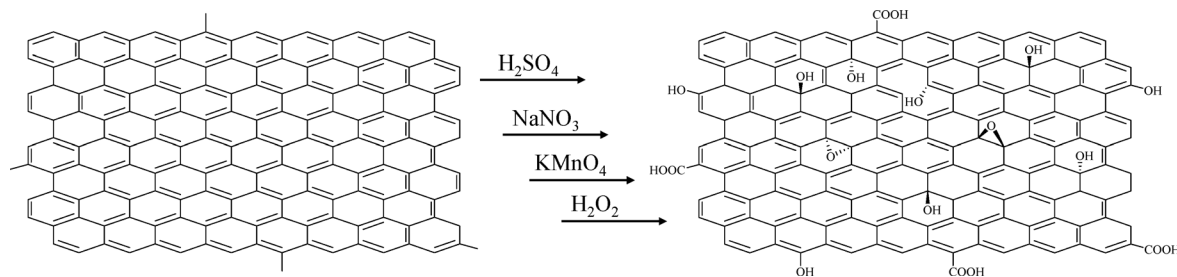


Fig. 2 Schematic of oxidation of graphene for form graphene oxide (GO).

X-Ray photoelectron spectroscopy

X-ray photoelectron spectroscopy (XPS) measurements were performed at the University of Michigan Center for Materials Characterization using a Kratos Axis Supra+ Instrument. The XPS measurements were performed on the Kratos Axis Supra+ system. The samples were probed with a monochromatic Al $K\alpha$ X-ray beam at 1.486 keV with the anode tuned to 15 kV and 20 mA. Photoelectrons were collected from an area $\sim 700 \mu\text{m} \times 300 \mu\text{m}$ at pass energies of 160 eV and 20 eV for survey and core scans respectively. The step size for spectral acquisition was set to 0.1 eV and 1 eV for core and survey scans respectively.

Results and discussion

The growth of layered assemblies using metal ion complexation chemistry requires several constituents, including appropriately functionalized supports and GO. The silicon and silica supports used in this work are characterized by surface silanol groups, which are reactive toward ClSO_3H . Preparation of the support surface requires cleaning and oxidation using piranha solution. For the silicon support, oxidation produces a *ca.* 15 Å surface oxide layer. Exposure of the oxidized and hydrolyzed supports to ClSO_3H produces a surface with a sufficiently high density of $\text{O}-\text{SO}_3^-$ functionalities for our purposes (Fig. 1). The change in the thickness from 15 Å to a higher value (measured ellipsometrically) confirmed the modification of the surfaces.

The functionalization of graphene to form GO is the first step in creating the primary layer component. GO is formed by the oxidation of graphene which is not an inherently chemically selective process. As noted in the Introduction, the oxidation of GO results in the presence of epoxide, alcohol, aldehyde and carboxylate functionalities, which are not expected to be

distributed in a fully random manner. The edges of the graphene sheets are expected to exhibit different reactivity toward oxidation than bonds located in the interior of the graphene sheet, and we schematize an oxidized GO sheet in Fig. 2.

The oxidation process results in the edge functionalities being primarily carboxylate/carboxylic acid, while the in-plane oxidized sites being characterized by a higher proportion of hydroxyl and epoxide groups. It is important to note that Fig. 2 is intended as a cartoon and not a quantitative depiction of the location or density of the various oxide species. The subsequent reaction of GO with chlorosulfonic acid produces a sulfated graphene oxide, where the hydroxyl groups on GO react with the ClSO_3H (Fig. 3). FTIR spectra of GO and S-GO are provided in the SI (Fig. S1).

With the sulfated support and S-GO in place, the formation of robust multilayers requires a species to connect the layers. The means of bonding the layer(s) of S-GO to the support and S-GO underlayers is metal ion complexation chemistry. This structural motif and the means used for inter-layer bonding is conceptually the same as so-called ZP layer growth chemistry.^{27–30,32–34,36–43,47,48} The exposure of a sulfate-functionalized support to the appropriate metal ion (Zr^{4+} here) results in rapid complexation of Zr^{4+} ions by surface-bound sulfate groups (Fig. 4). The deposition solution is 5 mM ZrOCl_2 in 60 : 40 ethanol : water.

With the support surface prepared as shown in Fig. 4, it is ready for deposition of S-GO sheets. S-GO is dissolved in MeCN (*ca.* $\sim 0.2 \text{ M}$) and the zirconated support is immersed in the solution (Fig. 5). By alternating deposition of Zr^{4+} and S-GO, multiple layers of S-GO can be deposited.

S-GO deposition times of two and four minutes were used and the recovered ellipsometric thickness (*vide infra*) of the

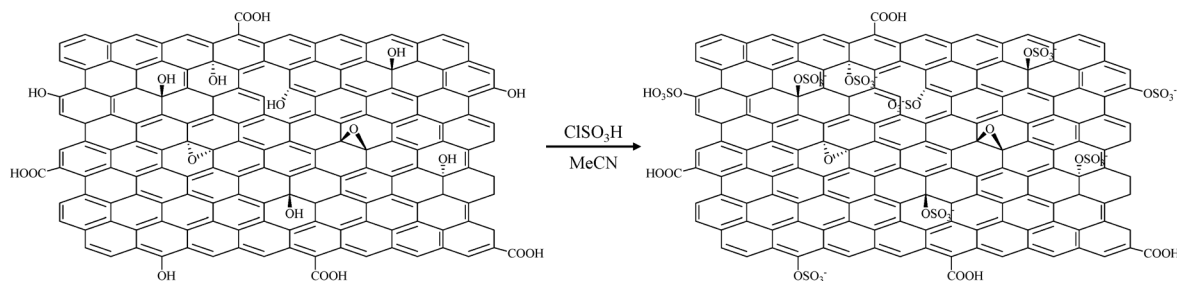


Fig. 3 Schematic of the reaction of GO with ClSO_3H to form sulfated graphene oxide (S-GO).



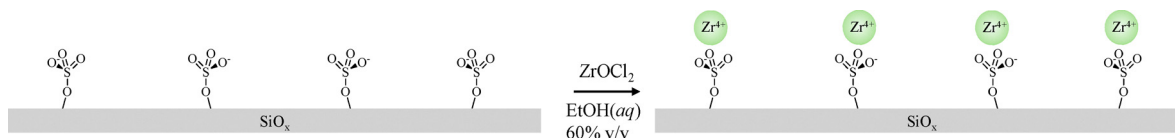


Fig. 4 Schematic of silica surface modification to form a sulfate-terminated interface. Spectator anionic species are not shown.

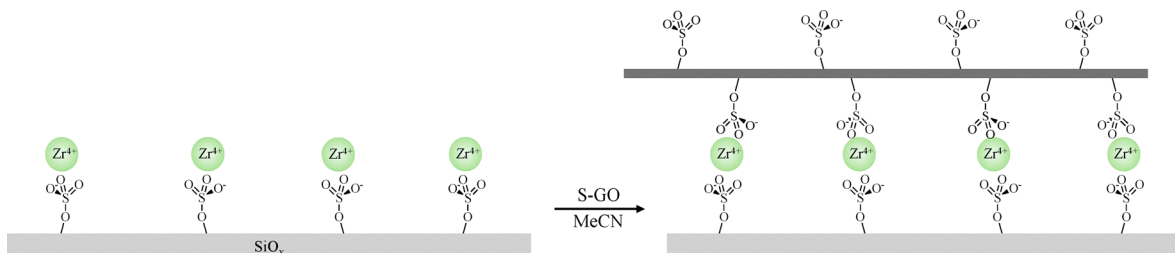


Fig. 5 Schematic of deposition of S-GO on a zirconated surface. Spectator anionic species are not shown.

S-GO adlayers was found to be the same for the two deposition times and to avoid repetition, only one data set has been reported (Fig. 7). For each S-GO deposition cycle, the Zr^{4+} deposition time was half that used for the S-GO.

Given the rapid kinetics of deposition of S-GO sheets, the nominally random distribution of OH (and thus $-\text{OSO}_3^-$) functionality of each S-GO sheet, and the amorphous nature of the SiO_x support surface, it is fair to consider whether full monolayer coverage can be achieved. We use optical ellipsometry to measure layer thickness and compare the ellipsometric results to the known estimated thicknesses of S-GO. GO is *ca.* 10 Å,⁵⁴ a $-\text{SO}_3^-$ group is taken to be 2.5 Å, and Zr^{4+} has an ionic radius of 0.9 Å. We estimate a layer thickness of *ca.* 16 Å (Fig. 6), which is the same to within the experimental uncertainty as the ellipsometric thickness (Fig. 7). (Ellipsometrically determined optical constants n and k are provided in Table S2 and Fig. S4) We have also constructed S-GO multilayers using hydroquinone bisulfate and for those multilayers

we expect a layer thickness of *ca.* 25 Å and obtain 27 Å ellipsometrically. Given the uncertainties in the thickness of the GO sheets and the assumptions inherent in the ellipsometric measurement, we consider this to be excellent agreement. While it is important to consider that the ellipsometric measurement averages over the spot size on the sample (several mm diameter) and cannot detect microscopic or nanoscopic heterogeneity, the correspondence between the molecular mechanics estimates and the ellipsometric data suggests that we obtain essentially full monolayer coverage for all deposition times tested and when an interlayer spacer is used. These results indicate that the kinetics of formation for the Zr-bissulfate interlayer linkage are fast, and that the thermodynamic driving force for layer growth is likely also strongly favorable based on the adlayer thickness data.

Related to the issue of coverage is the detailed nature of the ZS interlayer linkages. As noted above, the spatial distribution of GO sites that have been reacted to form sulfates is not

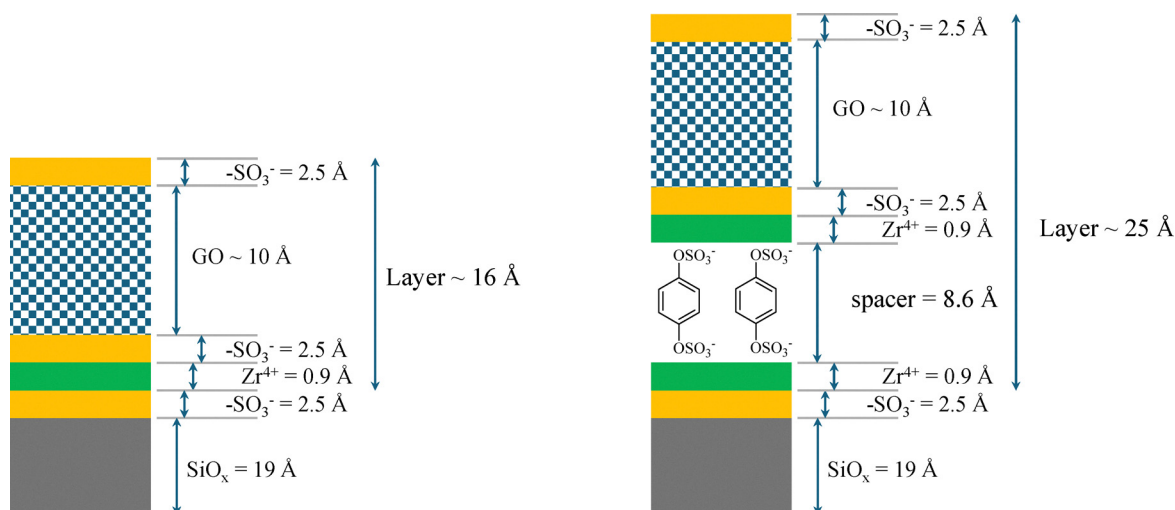


Fig. 6 Estimates of thickness per layer for S-GO layers linked directly between S-GO sheets (left) and linked with hydroquinone bisulfate spacers (right).



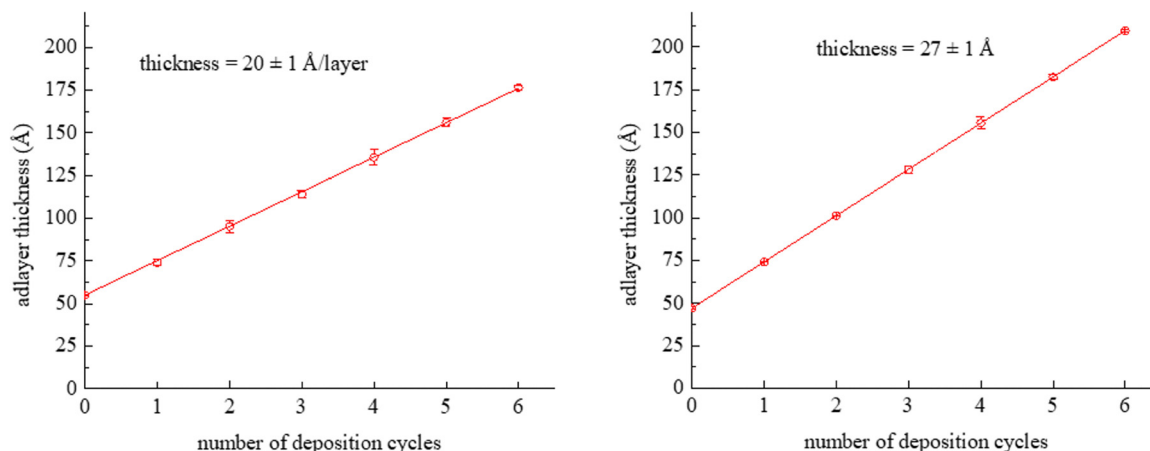


Fig. 7 Ellipsometric thickness per layer for S-GO layers linked directly between S-GO sheets (left) and linked with hydroquinone bisulfate spacers (right).

expected to be spatially regular, and a key question is the stoichiometric ratio of Zr:S and the approximate density of sulfate groups on the S-GO. We can address these issues using XPS. The XPS data are provided in SI, and are summarized in Tabular form in Table 1.

There is substantial useful information contained in the atomic concentration data. First, the ratio of S:Zr is $7.0_3 \pm 1.6_0$, indicating that not all of the sulfate functionalities participate in the ZS linking chemistry. The expected result for full participation would be either 2:1 with the presence of spectator ions, or 4:1 in the absence of spectator ions, so somewhere between 30 and 60% of the sulfate functionalities participate in interlayer bonding. This ratio also indicates that the association of Zr^{4+} with one sulfate is not seen, implying that the strength of interaction between one sulfate and Zr^{4+} is less than that of Zr^{4+} coordination with water, but the formation of the $\text{Zr}^{4+}(\text{O}_3\text{SO})_n$ complex ($n \geq 2$) is energetically more favorable. This finding stands in contrast to the result seen for the Zr-P-GO system. The oxygen in the system will be present either in the form of S-O or C-O bonds, and we know that with the reaction of GO with ClSO_3H sets the S:O ratio at 1:3 (the 4th oxygen for the sulfate is counted as a C-O). With that stoichiometric information and the atomic percentages of S and O (Table 1), we calculate that the C:O ratio is 3.9₄:1, indicating significant oxidation of graphene by ClSO_3H . This value is in reasonable agreement with the original report on the preparation of graphitic oxide, where the authors reported a C:O ratio

of 2.9:1.⁵⁵ We can further compare the atomic percentage of S to C, and find the C:S ratio is 3.7₁:1. The implication of this ratio is that ~94% of the oxidized sites of GO react with ClSO_3H .

The absorbance data for the direct ZS-linked S-GO adlayers deposited with two-minute and four-minute reaction times, and for the ZS-linked S-GO adlayers with hydroquinone bisulfate spacers with four-minute reaction time shown in Fig. 8 are all consonant with the ellipsometric data shown in Fig. 7. The absorbance data in Fig. 8 can be compared by measurement of the integrated area under the bands (220 nm–800 nm), because the band shape is seen to change slightly with the addition of layers. The step-like feature in the absorbance data at 350 nm (Fig. 8) is a result of the light source change and is not related to the adlayers. We report the integrated area under the absorbance bands rather than a simple absorbance maximum at *ca.* 230 nm. This is because of subtle changes in band shape with number of adlayers, which could indicate either a change in adlayer S-GO morphology with layer growth, or interlayer effects due to the extensive conjugation and the inherently parallel nature of these (conjugated) adlayers. The absorbance spectra of the adlayer assemblies with hydroquinone bisulfate spacers (Fig. 8e) exhibit the same adlayer-dependent variations in band shape, suggesting that interlayer interactions are not likely to fully explain the layer-dependence. The absorbance spectra of GO cannot be explained simply in the context of molecular spectra, and the integrated cross section is known to depend on the size of the GO sheet.⁵⁶ Thus, extracting quantitative information from these data is a challenge, but comparing the results for a given system as a function of number of adlayers is a useful gauge of growth, and that integrated areas is at least a qualitative gauge of the amount of S-GO present. With these caveats, the data in Fig. 8b, d and f show that the absorbance data are all consistent with the ellipsometric results (Fig. 7).

With both the ellipsometric and optical absorbance data being consistent with regular layer-by-layer growth, it is important to consider the morphology of these adlayers. We show in Fig. 9 SEM images of the adlayers. These layered assemblies

Table 1 XPS atomic concentrations (%) for Zr, S, C and O. Uncertainties are $\pm 1\sigma$

Sample	Zr 3d	S 2p	C 1s	O 1s
1a	1.4 \pm 0.1	8.0 \pm 0.2	29.3 \pm 0.4	33.7 \pm 0.2
1b	1.2 \pm 0.1	6.6 \pm 0.2	34.1 \pm 0.4	32.1 \pm 0.2
2a	1.1 \pm 0.1	6.0 \pm 0.2	38.8 \pm 0.4	32.3 \pm 0.2
2b	1.1 \pm 0.1	5.8 \pm 0.2	37.7 \pm 0.4	32.7 \pm 0.2
3a	0.9 \pm 0.1	10.1 \pm 0.3	26.1 \pm 0.5	26.9 \pm 0.2
3b	1.1 \pm 0.1	11.3 \pm 0.3	11.6 \pm 0.6	30.9 \pm 0.3
Average	1.1 ₃ \pm 0.2 ₄	7.9 ₇ \pm 0.5 ₈	29.6 ₀ \pm 1.1 ₂	31.4 ₃ \pm 0.5 ₄



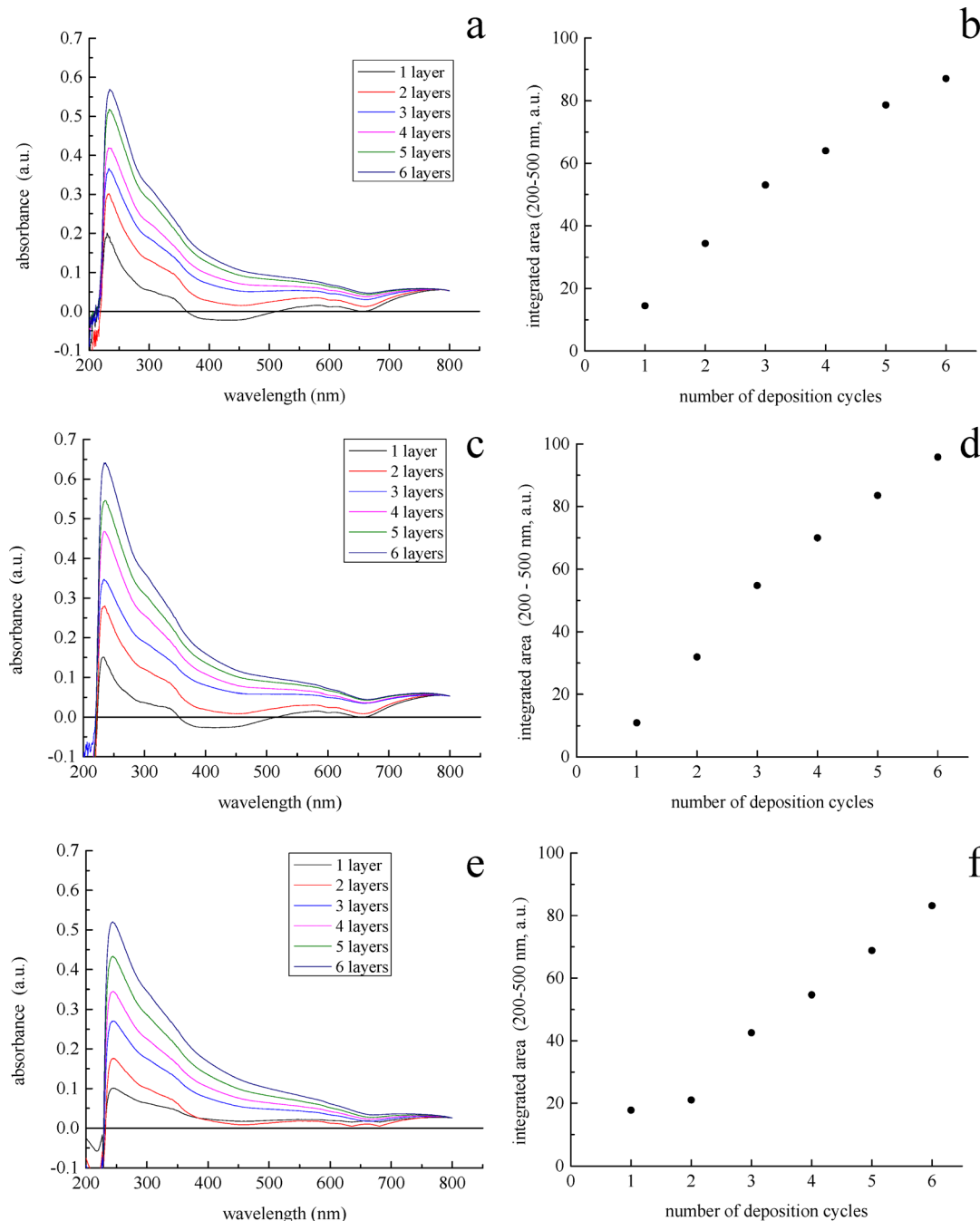


Fig. 8 (a): Absorbance spectra of direct ZS-linked S-GO adlayers for two-minute layer deposition reaction times. (b): integrated area under absorbance spectra (220–800 nm) for the spectra shown in (a) as a function of number of layers. (c): absorbance spectra of direct ZS-linked S-GO adlayers for four-minute layer deposition reaction time. (d): integrated area under absorbance spectra (220–800 nm) for the spectra shown in (c) as a function of number of layers. (e): absorbance spectra of direct ZS-linked S-GO adlayers with hydroquinone bisulfate spacers for four-minute layer deposition reaction time. (f): integrated area under absorbance spectra (220–800 nm) for the spectra shown in (e) as a function of number of layers.

exhibit what appear to be tiled deposition, which is an expected result. The image shown in Fig. 9a, for a two-minute deposition time appears to have somewhat different morphology than the four minute deposition time (Fig. 9b). Despite this visual difference, the ellipsometric (Fig. 7) and optical absorbance (Fig. 8) data yield the same results for the two deposition times.

Conclusions

We have reported the facile layer-by-layer growth of graphene oxide sulfate multilayer structures, with up to six layers, although there is no reason that these structures could be grown to more than six layers. The layers are bonded to a planar silica support using Zr^{4+} ions. Optical ellipsometry



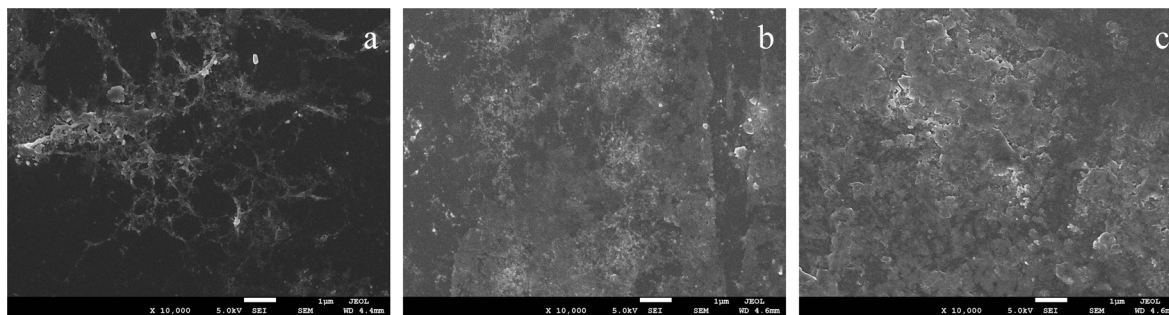


Fig. 9 SEM images of (a) six direct ZS-linked S-GO adlayers with two-minute layer deposition reaction times. (b) six direct ZS-linked S-GO adlayers with four-minute layer deposition reaction times. (c) six direct ZS-linked S-GO adlayers with hydroquinone bisulfate spacers with four-minute layer deposition reaction times. All images are 10 \times magnification, 5.0 kV acceleration voltage. Scale bars are 1 μ m.

shows step-by-step layer growth with layer thickness consistent with that expected from molecular mechanics calculations. The reaction to form Zr-bisulfate linkages is facile, with multistep layer deposition occurring within six to ten minutes per layer. The S-GO layers can be deposited directly on S-GO underlayer(s) or interlayer spacers (hydroquinone bisulfate was used here) can be incorporated to control the spacing with graphene oxide sulfate layers. The layer growth is rapid, with two minutes reaction time for zirconation and spacer deposition reactions producing fully reacted surfaces, and two-minute deposition time of S-GO producing the same result as four-minute deposition time. The XPS data give valuable information on the Zr-sulfate chemistry. The ZS interactions appear to be sufficiently favorable energetically to exclude excess water trapped in the GO layers, thus showing the robustness of these interactions. The SEM data show what appear to be “tiled” multilayer structures. This is the first report we are aware of that demonstrates rapid and robust layer-by-layer growth of graphene oxide structures.

Conflicts of interest

There are no conflicts to declare.

Data availability

All data used in this work will be made available to any interested party. Please contact the corresponding author to obtain the data.

FTIR spectra and band assignments for GO and S-GO, XPS spectra of the S-GO samples, ellipsometrically determined optical constants. See DOI: <https://doi.org/10.1039/d5ma00601e>

Acknowledgements

This material is based upon work supported by the US. Department of Energy's Office of Energy Efficiency and Renewable Energy (EERE) under the Hydrogen and Fuel Cell Technologies Office Award Number DE-EE0011106. The authors acknowledge the University of Michigan College of Engineering for financial

support and the Michigan Center for Materials Characterization for use of the instruments and staff assistance.

References

- 1 F. Gao, S. Zhang, Q. Lv and B. Yu, Recent advances in graphene oxide catalyzed organic transformations, *Chin. Chem. Lett.*, 2022, **33**, 2354–2362.
- 2 Y. Yan, W. I. Shin, H. Chen, S.-M. Lee, S. Manickam, S. Hanson, H. Zhao, E. Lester, T. Wu and C. H. Pang, A recent trend: application of graphene in catalysis, *Carbon Lett.*, 2021, **31**, 177–199.
- 3 C. Su, M. Acik, K. Takai, J. Lu, S.-J. Hao, Y. Zheng, P. Wu, Q. Bao, T. Enoki, Y. J. Chabal and K. Ping Loh, Probing the catalytic activity of porous graphene oxide and the origin of this behaviour, *Nat. Commun.*, 2012, **3**, 1298.
- 4 P. Tang, G. Hu, M. Li and D. Ma, Graphene-Based Metal-Free Catalysts for Catalytic Reactions in the Liquid Phase, *ACS Catal.*, 2016, **6**, 6948–6958.
- 5 L. Shang, Y. Qi, H. Lu, H. Pei, Y. Li, L. Qu, Z. Wu and W. Zhang, in *Theranostic Bionanomaterials*, ed. W. Cui and X. Zhao, Elsevier, 2019, pp. 165–185, DOI: [10.1016/B978-0-12-815341-3.00007-9](https://doi.org/10.1016/B978-0-12-815341-3.00007-9).
- 6 R. Geetha Bai, K. Muthoosamy, S. Manickam and A. Hilal-Alnaqbi, Graphene-based 3D scaffolds in tissue engineering: fabrication, applications, and future scope in liver tissue engineering, *Int. J. Nanomed.*, 2019, **14**, 5753–5783.
- 7 S. R. Shin, Y.-C. Li, H. L. Jang, P. Khoshakhlagh, M. Akbari, A. Nasajpour, Y. S. Zhang, A. Tamayol and A. Khademhosseini, Graphene-based materials for tissue engineering, *Adv. Drug Delivery Rev.*, 2016, **105**, 255–274.
- 8 K. Zhihui and D. Min, Application of Graphene Oxide-Based Hydrogels in Bone Tissue Engineering, *ACS Biomater. Sci. Eng.*, 2022, **8**, 2849–2857.
- 9 N. Bellier, P. Baipaywad, N. Ryu, J. Y. Lee and H. Park, Recent biomedical advancements in graphene oxide- and reduced graphene oxide-based nanocomposite nanocarriers, *Biomater. Res.*, 2022, **26**, 65.
- 10 C. Chung, Y.-K. Kim, D. Shin, S.-R. Ryoo, B. H. Hong and D.-H. Min, Biomedical Applications of Graphene and Graphene Oxide, *Acc. Chem. Res.*, 2013, **46**, 2211–2224.



- 11 S. Patil, C. Rajkubera and S. Sagadevan, Recent biomedical advancements in graphene oxide and future perspectives, *J. Drug Delivery Sci. Technol.*, 2023, **86**, 104737.
- 12 M. Mehta, R. Gadhvi, G. Shah and V. N. Mehta, in *Comp. Anal. Chem.*, ed. S. K. Kailasa, Elsevier, 2024, vol. 106, pp. 629–651.
- 13 Y. Zhu, S. Murali, W. Cai, X. Li, J. W. Suk, J. R. Potts and R. S. Ruoff, Graphene and Graphene Oxide: Synthesis, Properties, and Applications, *Adv. Mater.*, 2010, **22**, 3906–3924.
- 14 D. L. Allara and R. G. Nuzzo, Spontaneously organized molecular assemblies. 2. Quantitative infrared spectroscopic determination of equilibrium structures of solution-adsorbed n-alkanoic acids on an oxidized aluminum surface, *Langmuir*, 1985, **1**, 52–66.
- 15 A. Holm, C. J. Wrasman, K.-C. Kao, A. R. Riscoe, M. Cargnello and C. W. Frank, Langmuir–Blodgett Deposition of Graphene Oxide—Identifying Marangoni Flow as a Process that Fundamentally Limits Deposition Control, *Langmuir*, 2018, **34**, 9683–9691.
- 16 K. Bandyopadhyay, V. Patil, K. Vijayamohan and M. Sastry, Adsorption of Silver Colloidal Particles through Covalent Linkage to Self-Assembled Monolayers, *Langmuir*, 1997, **13**, 5244–5248.
- 17 I. Langmuir, The Constitution and Fundamental Properties of Solids and Liquids. II. Liquids, *J. Am. Chem. Soc.*, 1917, **39**, 1848–1906.
- 18 K. B. Blodgett, Films Built by Depositing Successive Monomolecular Layers on a Solid Surface, *J. Am. Chem. Soc.*, 1935, **57**, 1007–1022.
- 19 L. Netzer, R. Iscovici and J. Sagiv, Adsorbed monolayers versus Langmuir–Blodgett monolayers – why and how? II. Characterization of built-up films constructed by stepwise adsorption of individual monolayers, *Thin Solid Films*, 1983, **100**, 67–76.
- 20 L. Netzer, R. Iscovici and J. Sagiv, Adsorbed monolayers versus Langmuir–Blodgett monolayers - why and how? I. From monolayer to multilayer, by adsorption, *Thin Solid Films*, 1983, **99**, 235–241.
- 21 L. Netzer and J. Sagiv, A new approach to construction of artificial monolayer assemblies, *J. Am. Chem. Soc.*, 1983, **105**, 674–676.
- 22 J. Sagiv, Organized monolayers by adsorption. III. Irreversible adsorption and memory effects in skeletonized silane monolayers, *Isr. J. Chem.*, 1979, **18**, 346–353.
- 23 J. Sagiv, Organized monolayers by adsorption. II. Molecular orientation in mixed dye monolayers built on anisotropic polymeric surfaces, *Isr. J. Chem.*, 1979, **18**, 339–345.
- 24 J. Sagiv, Organized monolayers by adsorption. 1. Formation and structure of oleophobic mixed monolayers on solid surfaces, *J. Am. Chem. Soc.*, 1980, **102**, 92–98.
- 25 J. Sagiv and E. E. Polymeropoulos, Adsorbed Monolayers. Molecular Organization and Electrical Properties, *Ber. Bunsen-Ges. Phys. Chem.*, 1978, **82**, 883.
- 26 P. Kohli and G. J. Blanchard, Applying Polymer Chemistry to Interfaces: Layer-by-Layer and Spontaneous Growth of Covalently Bound Multilayers, *Langmuir*, 2000, **16**, 4655–4661.
- 27 H. E. Katz, G. Scheller, T. M. Putvinski, M. L. Schilling, W. L. Wilson and C. E. D. Chidsey, Polar Orientation of Dyes in Robust Multilayers by Zirconium Phosphate-Phosphonate Interlayers, *Science*, 1991, **254**, 1485–1487.
- 28 H. Lee, L. J. Kepley, H. G. Hong and T. E. Mallouk, Inorganic analogs of Langmuir–Blodgett films: adsorption of ordered zirconium 1,10-decanebisphosphonate multilayers on silicon surfaces, *J. Am. Chem. Soc.*, 1988, **110**, 618–620.
- 29 H. Lee, L. J. Kepley, H. G. Hong, S. Akhter and T. E. Mallouk, Adsorption of ordered zirconium phosphonate multilayer films on silicon and gold surfaces, *J. Phys. Chem.*, 1988, **92**, 2597–2601.
- 30 E. H. Yonemoto, G. B. Saupe, R. H. Schmehl, S. M. Hubig, R. L. Riley, B. L. Iverson and T. E. Mallouk, Electron-Transfer Reactions of Ruthenium Trisbipyridyl-Viologen Donor-Acceptor Molecules: Comparison of the Distance Dependence of Electron Transfer-Rates in the Normal and Marcus Inverted Regions, *J. Am. Chem. Soc.*, 1994, **116**, 4786–4795.
- 31 H. C. Yang, K. Aoki, H. G. Hong, D. D. Sackett, M. F. Arendt, S. L. Yau, C. M. Bell and T. E. Mallouk, Growth and characterization of metal(II) alkanebisphosphonate multilayer thin films on gold surfaces, *J. Am. Chem. Soc.*, 1993, **115**, 11855–11862.
- 32 G. Cao, L. K. Rabenberg, C. M. Nunn and T. E. Mallouk, Formation of quantum-size semiconductor particles in a layered metal phosphonate host lattice, *Chem. Mater.*, 1991, **3**, 149–156.
- 33 D. Rong, H.-G. Hong, Y. I. Kim, J. S. Krueger, J. E. Mayer and T. E. Mallouk, Electrochemistry and photoelectrochemistry of transition metal complexes in well-ordered surface layers, *Coord. Chem. Rev.*, 1990, **97**, 237–248.
- 34 M. E. Thompson, Use of Layered Metal Phosphonates for the Design and Construction of Molecular Materials, *Chem. Mater.*, 1994, **6**, 1168–1175.
- 35 L. A. Vermeulen and M. E. Thompson, Stable photoinduced charge separation in layered viologen compounds, *Nature*, 1992, **358**, 656–658.
- 36 L. A. Vermeulen, J. L. Snover, L. S. Sapochak and M. E. Thompson, Efficient photoinduced charge separation in layered zirconium viologen phosphonate compounds, *J. Am. Chem. Soc.*, 1993, **115**, 11767–11774.
- 37 J. L. Snover, H. Byrd, E. P. Suponeva, E. Vicenzi and M. E. Thompson, Growth and Characterization of Photoactive and Electroactive Zirconium Bisphosphonate Multilayer Films, *Chem. Mater.*, 1996, **8**, 1490–1499.
- 38 H. E. Katz, W. L. Wilson and G. Scheller, Chromophore Structure, Second Harmonic Generation, and Orientational Order in Zirconium Phosphonate/Phosphate Self-Assembled Multilayers, *J. Am. Chem. Soc.*, 1994, **116**, 6636–6640.
- 39 H. E. Katz, S. F. Bent, W. L. Wilson, M. L. Schilling and S. B. Ungashe, Synthesis Layer Assembly, and Fluorescence Dynamics of Poly(phenylenevinylene) Oligomer Phosphonates, *J. Am. Chem. Soc.*, 1994, **116**, 6631–6635.
- 40 S. B. Ungashe, W. L. Wilson, H. E. Katz, G. R. Scheller and T. M. Putvinski, Synthesis, self-assembly, and photophysical dynamics of stacked layers of porphyrin and viologen phosphonates, *J. Am. Chem. Soc.*, 1992, **114**, 8717–8719.



- 41 H. E. Katz, M. L. Schilling, C. E. D. Chidsey, T. M. Putvinski and R. S. Hutton, Quaterthiophenediphosphonic acid (QDP): a rigid, electron-rich building block for zirconium-based multilayers, *Chem. Mater.*, 1991, **3**, 699–703.
- 42 T. M. Putvinski, M. L. Schilling, H. E. Katz, C. E. D. Chidsey, A. M. Mujsce and A. B. Emerson, Self-assembly of organic multilayers with polar order using zirconium phosphate bonding between layers, *Langmuir*, 1990, **6**, 1567–1571.
- 43 H. E. Katz, Multilayer Deposition of Novel Organophosphonates with Zirconium(IV), *Chem. Mater.*, 1994, **6**, 2227–2232.
- 44 H. Byrd, S. Whipps, J. K. Pike, J. Ma, S. E. Nagler and D. R. Talham, Role of the template layer in organizing self-assembled films: zirconium phosphonate monolayers and multilayers at a Langmuir-Blodgett template, *J. Am. Chem. Soc.*, 1994, **116**, 295–301.
- 45 H. Byrd, J. K. Pike and D. R. Talham, Inorganic monolayers formed at an organic template: a Langmuir-Blodgett route to monolayer and multilayer films of zirconium octadecylphosphonate, *Chem. Mater.*, 1993, **5**, 709–715.
- 46 P. Kohli and G. J. Blanchard, Design and Growth of Robust Layered Polymer Assemblies with Molecular Thickness Control, *Langmuir*, 1999, **15**, 1418–1422.
- 47 J. C. Horne, Y. Huang, G. Y. Liu and G. J. Blanchard, Correspondence between Layer Morphology and Intralayer Excitation Transport Dynamics in Zirconium–Phosphonate Monolayers, *J. Am. Chem. Soc.*, 1999, **121**, 4419–4426.
- 48 J. C. Horne and G. J. Blanchard, Structural Mediation of Interlayer Excitation Transport in Zirconium–Phosphonate Multilayers, *J. Am. Chem. Soc.*, 1999, **121**, 4427–4432.
- 49 F.-X. Xiao, M. Pagliaro, Y.-J. Xu and B. Liu, Layer-by-layer assembly of versatile nanoarchitectures with diverse dimensionality: a new perspective for rational construction of multilayer assemblies, *Chem. Soc. Rev.*, 2016, **45**, 3088–3121.
- 50 M. Yang, Y. Hou and N. A. Kotov, Graphene-based multilayers: Critical evaluation of materials assembly techniques, *Nano Today*, 2012, **7**, 430–447.
- 51 S. W. Keller, S. A. Johnson, E. S. Brigham, E. H. Yonemoto and T. E. Mallouk, Photoinduced Charge Separation in Multilayer Thin Films Grown by Sequential Adsorption of Polyelectrolytes, *J. Am. Chem. Soc.*, 1995, **117**, 12879–12880.
- 52 S. B. Bakiemoh and G. J. Blanchard, Demonstration of Oriented Multilayers through Asymmetric Metal Coordination Chemistry, *Langmuir*, 1999, **15**, 6379–6385.
- 53 H. A. Becerril, J. Mao, Z. Liu, R. M. Stoltenberg, Z. Bao and Y. Chen, Evaluation of Solution-Processed Reduced Graphene Oxide Films as Transparent Conductors, *ACS Nano*, 2008, **2**, 463–470.
- 54 I. Jung, M. Vaupel, M. Pelton, R. Piner, D. A. Dikin, S. Stankovich, J. An and R. S. Ruoff, Characterization of Thermally Reduced Graphene Oxide by Imaging Ellipsometry, *J. Phys. Chem. C*, 2008, **112**, 8499–8506.
- 55 W. S. Hummers, Jr. and R. E. Offeman, Preparation of Graphitic Oxide, *J. Am. Chem. Soc.*, 1958, **80**, 1339.
- 56 T. Zhang, G.-Y. Zhu, C.-H. Yu, Y. Xie, M.-Y. Xia, B.-Y. Lu, X. Fei and Q. Peng, The UV absorption of graphene oxide is size-dependent: possible calibration pitfalls, *Microchim. Acta*, 2019, **186**, 207.

